

Modeling Ring Currents in a Planeterrella Device

by

E. R. Ayari

Bachelor of Science – Department of Physics

Undergraduate Honors Thesis

Defense Copy

Thesis Defense Committee:

Mihály Horányi	Advisor	Department of Physics
Prof. John Cumalat	Honors Council Representative	Department of Physics
Prof. Zoltan Sternovsky	External Faculty Member	Department of Aerospace Engineering Science

To defend on:

March 24th, 2021

This thesis entitled:
Modeling Ring Currents in a Planeterrella Device
written by E. R. Ayari
has been approved for the Department of Physics

Prof. Mihály Horányi

Prof. John Cumalat

Prof. Zoltan Sternovsky

Date _____

The final copy of this thesis has been examined by the signatories, and we find that both the content and the form meet acceptable presentation standards of scholarly work in the above mentioned discipline.

Ayari, E. R. (B.A., Physics)

Modeling Ring Currents in a Planeterrella Device

Thesis directed by Prof. Mihály Horányi

Studying the dynamics of plasmas confined within dipole magnetic fields gives insight into how planetary magnetospheres behave and evolve over time. In order to perform diagnostics on such a plasma, a Runge-Kutta based collision algorithm was developed to follow the motions of electrons within a dipole field and track their collisions with neutral N₂ and O₂ particles. Alongside theoretical modeling, a laboratory Planeterrella setup, manufactured at the Institute for Modeling Plasmas and Cosmic dust within the Laboratory for Atmospheric and Space Physics (IMPACT/LASP), is used to study the dynamics of trapped electrons through light emission generated by impact excitation, ionization, and recombination processes. Light images from the Planeterrella setup are used to derive the motion of electrons in a dipole field as they collide with neutral atoms. The duality of simulation and experiment reveals more information about the dynamics of trapped electrons.

Dedication

To my family and LASP.

Acknowledgements

First, I would like to express my gratitude to Dr. Mihály Horányi for hiring me to work at the Institute for Modeling Plasma, Atmospheres and Cosmic Dust (IMPACT) at LASP, as well as being my advisor for this honors thesis. In addition, I would like to thank Dr. Jan Deca very much for introducing me to the art of plasma simulations, and answering my endless questions. Thanks also to Dr. Xu Wang for serving as the experimental advisor for this thesis. Finally, I would like to thank John Fontanese, Alex Doner and Thomas Watts for helping set up the physical experiments.

Contents

Chapter

1	Introduction	1
2	Motivation for Studying Ring Currents	5
2.1	Ring current research questions	6
2.2	Heritage of the Planeterrella	7
2.3	Modern Planeterrellas	7
3	Motion of Charged Particles in Electric and Magnetic Fields	9
3.1	The Lorentz force and pertinent plasma parameters	9
3.2	Guiding center particle drifts	10
3.2.1	$\vec{E} \times \vec{B}$ drift	11
3.2.2	Magnetic gradient ($\nabla \vec{B}$) drift	11
3.2.3	Magnetic curvature drift	12
3.3	Magnetic dipole fields	12
4	Collisional Phenomena	15
4.1	Key parameters	15
4.2	Impact excitation	17
4.3	Excitations	18
4.3.1	Rotational excitations	18

5	Construction of the Experimental Apparatus	20
5.1	SolidWorks model	20
5.2	Mechanical fabrication	21
5.3	Electric system	22
6	Simulation	25
6.1	Runge-Kutta numerical integration	25
6.2	Python implementation	25
6.3	Simulation modeling of electron-impact excitation collisions	26
6.3.1	Modeling photon emissions	28
6.4	Parallelization	29
6.5	Collision density analysis	30
6.6	Image luminosity analysis	31
7	Results	32
7.1	Simulation results	32
7.2	Experimental results	37
8	Conclusion	39
8.1	Summary of Findings	39
8.2	Further research	40
8.2.1	Spectra based on different gas compositions	40
8.2.2	Tilted dipole field	40
8.2.3	Improvements to the simulation	40
8.3	Glow Discharge	41
8.4	Research performed concurrently with this honors thesis	41
Bibliography		43

Tables

Table

Figures

Figure

2.1	Bernard's experimental Planeterrella results for modeling the Martian atmosphere. Note the blue color and orientation of the produced aurora.	8
3.1	Depiction of guiding center drift due to perpendicular electric and magnetic fields. Here, the magnetic field is oriented into the page, and the electric field is oriented to the right. The direction of the guiding center motion is denoted by v_{gc} . [7] . . .	11
3.2	Charged particle motion about the Earth. The ring current motion due to curvature and gradient drifts closer to the Earth for ions and electrons is indicated, as well as gyration about magnetic field lines and bounce motion between polar magnetic mirror points. Credit: NASA/GSFC	14
4.1	Representations of the density, cross section and mean free path length for an arbi- trary particle species.	16
4.2	Artist's rendering of a quantum rigid rotor. For the N ₂ and O ₂ molecules within the Planeterrella, $m_1 = m_2$. Here, c.ofm. is short for the center of mass, and the orientation of the quantum total angular momentum J is indicated.	19
5.1	a) Aluminum baseplate diagram of the Planeterrella apparatus and b) Solidworks rendering of the bell jar, vacuum seal and the baseplate of the Planeterrella apparatus.	20
5.2	The two mating aluminum hemispheres.	21
5.3	Linear and rotary position adjustment of the magnet.	22

5.4 a) Vacuum system diagram and b) Implemented vacuum system.	22
5.5 Schematics of the electric connections.	23
5.6 Auxiliary components in the electrical system.	24
6.1 Simulation result for a particle gyrating along a magnetic field line, exhibiting bounce motion between two mirror points.	27
6.2 Illustration of the multiprocessing algorithm when implemented over 8 cores. Credit: Konstantin Taletskiy, towardsdatascience.com	30
6.3 Density estimate results.	31
7.1 3D collision profile for the ring currents. The black point represents the center of the magnetic dipole field. The gaps on the left and right hand side ($x = \pm 10$) are an artifact of the random numbers used to generate the y-values of both the positions and velocities of the radial distributions.	33
7.2 2D density profile example for the stellar ring currents. The gaps on the left and right hand side ($x = \pm 10$) are an artifact of the random numbers used to generate the y-values of both the positions and velocities of the radial distributions. The histograms appearing on the opposite sides of the x and y axes represent probability distributions for the collisions based on location.	34
7.3 2D average velocity distribution for up to 15cm from the center of the sphere. This is meant to represent a birds-eye view of the Planeterrella in a centimeter scale, where the colorbar represents the average velocity of particles in a given location. The uniformity in the data from 4-6cm and 8-12cm corresponds to the location of the rings. Note also that the scale is given in 10^4 m/s for better presentation.	35
7.4 2D average distribution of cyclotron frequency to collision frequency for up to 15cm from the center of the sphere. Here, the ratio is indicated by the color. This is again meant to represent a birds-eye view of the Planeterrella in a centimeter scale.	36
7.5 N2 ring current result at 1600 Volts.	38

Chapter 1

Introduction

Plasma Physics is a field of research that seeks to understand the fourth state of matter. A *plasma* is a gas that has been sufficiently heated to where atoms and electrons collide with enough energy to knock electrons off of neutral atoms, giving them a positive net charge. This process of a neutral atom losing an electron and gaining a positive net charge is called *ionization*. Due to the long-range Coulomb forces between charged particles, even a partially ionized plasma can exhibit collective behavior leading to waves and instabilities.

A Planeterrella is a device used to visualize collisional plasmas via a biased and magnetized sphere within a cylindrical or spherical vacuum chamber. Its earliest prototype, dubbed the Terrella, was first developed by Norwegian physicist Kristian Birkeland in 1901 to recreate the Aurora Borealis (Northern Lights) he witnessed during an expedition to the Norwegian Polar region. The term *Terrella* was first coined by British physicist William Gilbert, who used it to describe a spherical magnet representing Earth[11]. Today, there are far more accurate existing Terrella setups being used for research and teaching purposes throughout the world, including at the Institute for Modeling Plasmas, Atmospheres, and Cosmic Dust (IMPACT) of the Laboratory for Atmospheric and Space Physics (LASP) at the University of Colorado Boulder. The way the Planeterrella at IMPACT operates is that the air within the chamber is pumped down via a vacuum pump to pressures on the order of 400 mTorr, and a -2 kV bias potential is applied to an aluminum sphere with a 0.5 Tesla bar magnet embedded within it. When the bias is applied, free electrons are repelled radially from the sphere but trapped within the dipole magnetic field, yielding regions of

high electron-electron and electron-neutral collision densities within the vicinity of the sphere. For this reason, the presence of visible glow may indicate regions where the electron-neutral collision density is sufficiently high, leading to impact excitation, ionization and recombination.

The results described in Chapter 7 show that the visible glow mainly arises from photo-emission due to impact excitation, in which a free electron that has enough incident energy to exceed a neutral atom's ionization energy collides with the atom. After the collision a valence electron is lost from the atom, leaving it in an ionized and excited metastable state [7]. This metastable state generally has a lifetime of ~ 10 nanoseconds, unless the excited ion collides with another electron. In either case, a photon is emitted from the atom, returning it to its ground state. In the case where a free electron collides with the excited ion, it returns the atom to its neutral state by combining with it in a process called *radiative recombination* [8]. The energy of the emitted photon is given by the difference between the ground and excited state energies. For this system, impact excitation processes can be thought of as the “source” of ions, whereas recombination is the “sink”.

The device at IMPACT is contained within a custom bell jar and vacuum seal, both of which were ordered from the vacuum science company Kurt J. Lesker. Within this bell jar is an aluminum sphere on a stand with a plastic support tube. The sphere and its stand are biased via a high voltage power supply. The sphere is surrounded by a strong magnetic dipole field due to the .5 Tesla bar magnet embedded within it. The entire system rests on an aluminum base plate, with the wiring, the pump, vacuum gauge and power supply beneath it. This apparatus has been shown to simulate various planetary and stellar visible plasma phenomena such as coronal expansion, the magnetopause, and auroral ovals by altering the applied voltage, pressure and geometry of the system, including the orientation of the embedded permanent magnet inside. This paper focuses on the physics behind the formation of ring currents.

When ring currents are generated by the Planeterrella, most frequently there are two distinct rings. The primary ring is closer to the sphere and more luminous, while the second ring is further from the sphere and less bright. Moreover, the primary ring appears purple and thin while the

secondary ring is red and has more spread. The objective of the project is to understand the processes responsible for the formation of these rings, their geometry and their color. To this end, a Runge-Kutta-based numerical Monte-Carlo Collision (MCC) simulation code was developed. In addition, experiments were done with the device, so that birds-eye imagery of the ring currents could be analyzed and compared to the numerical simulation results. The validity of the modeling effort was tested by pumping down the chamber to 5 ± 2.5 mTorr, refilling it with N₂ gas to a pressure of 500 ± 2.5 mTorr, and finally pumping back down to 5 ± 2.5 mTorr to reach a composition of $96 \pm 3.5\%$ of N₂, and only witnessing one ring.

The ring currents' light is generated due to the electrons experiencing $\vec{E} \times \vec{B}$, magnetic field gradient and curvature drifts [7]. These drifts arise from the perpendicular orientation of the electric and magnetic fields, as well as the spatial variation of the magnetic field. The electrons are trapped within this magnetic field and orbit the sphere in a counter-clockwise motion when observed from above. This trapping occurs when charged particles (such as protons or electrons) from some source gyrate about field lines, oscillate between two magnetic mirror points, and drift around the center of the field. The ring currents, due to the combination of drifts, form around the equator of the sphere and are visible within the Planeterrella due to the collision-based photon emissions processes. Collisions are the most common momentum transport process in the device due to the modest vacuum conditions resulting in high rates of energetic collisions in the contained plasma.

These MCC methods are shown to be accurate in tracking collisions for a plasma with similar temperature to the Planeterrella [3]. Since the number of collisions is proportional to the temperature by a factor of \sqrt{T} , the MCC method can accurately describe the one responsible for creating the ring currents. Numerical methods are used to integrate a Lorentz-Force-based equation of motion for an electron over a set number of time steps. The parameters of the plasma and a uniform random number are used to estimate when and where a collision occurs. This showed two distinct rings of collisions when displayed based on the ionization energy of the neutral. This simulation was successfully able to characterize the geometry of the rings based on mapping regions by the

ratio of collision and cyclotron frequencies. The methods developed in this work can be extended to arbitrary magnetic field configurations.

Chapter 2

Motivation for Studying Ring Currents

This chapter describes the significance of and motivation for studying ring currents (and other atmospheric plasma phenomena) within a Planeterrella. The underlying reason behind the formation of ring currents is the confinement of charged particles within a magnetic dipole field. Confinement of charged particles in a magnetic field is a common area of study across different disciplines of Physics, from the confinement of ultra-hot plasmas in fusion devices to the confinement of ions for quantum computing purposes. For ring currents, particles are trapped between the strong magnetic regions surrounding the North and South poles of the planetary object they are orbiting. This process in which charged particles are forced to oscillate between two regions where the magnetic field is strong is called *magnetic mirroring*. Magnetic mirroring effects are discussed more in depth in Chapter 3. Early studies using the Terrella revealed groundbreaking discoveries regarding the magnetism of the Earth such as why compass needles point North. The compass needle discovery was made by Queen Elizabeth I's royal physician William Gilbert. Gilbert demonstrated his early theories of magnetism by constructing a "Terrella" out of lodestone and showing that a compass changing its orientation about the Terrella exhibited identical behavior to that of one around the Earth [11]. Today, new Terrella configurations such as "La Planeterrella" located at the French Institute of Planetology and Astrophysics in Grenoble (IPAG) are being used to make new discoveries about the dynamics of charged particles, and the formation of the so-called radiation belts of planets with magnetic fields [6].

2.1 Ring current research questions

How do ring currents form?

Since ring currents are very common throughout the solar system, the initial conditions that lead to their formation is a topic of interest. Planets besides Earth have very different magnetic fields, so the processes by which they trap particles is also of interest. For example, Jupiter's magnetosphere is approximately 1000 times more voluminous than that of Earth and has significantly more energetic particles in its radiation belts. [14]

How do Stellar Ring Currents affect humans?

By studying properties of laboratory plasmas, we can better understand the naturally occurring plasmas in space. A physical example of ring currents and a prominent research topic are the Van Allen Radiation Belts. The Van Allen Belts are formed by the trapping of charged particles within Earth's magnetic dipole field [7]. Dipole fields and trapping of charged particles are discussed further in depth in chapter 3. Part of why the Van Allen Belts are so frequently studied is the presence of geomagnetic storms. These are disturbances in Earth's Magnetosphere due to fluctuations in the intensity and speed of the solar wind approaching Earth. Understanding these storms is essential because the precipitating and heated electrons produced by these storms can endanger satellites. The hot electrons can also cause perturbations in the ionosphere that interfere with radio and GPS signals[12]. In addition, geomagnetic storms produce changes in the Aurora Borealis (Northern Lights) and can create harmful geomagnetic induced currents (GICs) in the power grid and pipelines [12]. By understanding the dynamics of stellar ring currents we can better predict the behavior and effects of these storms.

How are ring currents studied on a larger scale?

In addition to the larger scale Terrella being used for research at the University of Iowa [2], stellar ring currents also play a significant role in atmospheric science. The higher energy particles in

orbit within the Van Allen Belts produce a net magnetic field in opposition to the Earth's. This negatively oriented magnetic field effect is measured by the disturbance storm time (Dst) index. The Dst index is a globally-averaged magnetic perturbation [12] and is an accurate representation of geomagnetic storm intensities.

2.2 Heritage of the Planeterrella

Kristian Birkeland (1867-1917) was part of a movement of physicists who extrapolated early ideas of Plasma Physics from J.J. Thompson's discovery of the electron in 1897. Birkeland is well known for his discoveries made in geophysics and the plasma surrounding the Earth by experimenting with laboratory gas discharges. His initial theory regarding the origin of Polar Aurora was that it was produced by cathode rays attracted to Earth's magnetic poles, since he was able to simulate the aurora within the laboratory by using a cathode ray and a dipole magnet [11]. A cathode ray is an electron beam emitted from a high-vacuum tube's cathode. After issuing his hypothesis in 1896, Birkeland traveled to the Norwegian North Pole to better understand Geophysics, Polar Aurora and Planetary Rings.

Størmer's calculations for the motion of a charged particle in a magnetic dipole field were the basis of many of Birkeland's theories regarding the Aurora. Størmer's significant contribution to this physics was that he showed the radius of curvature of any particle's path, or the *Størmer radius* is proportional to the square of its distance from the center of the magnetic dipole. This finding implied the presence of *forbidden regions* in Earth's magnetosphere, where charged particles from solar wind could not reach [10]. More of Størmer's findings are discussed in section 3.3.

2.3 Modern Planeterellas

The "La Planeterella" in France [6] has been used to simulate the Aurora produced by the magnetic anomalies surrounding Mars . In January of 2015 the NASA mission *Mars Atmosphere*

and Volatile Evolution mission (MAVEN) confirmed the presence of Ultraviolet (UV) radiation in the Martian Atmosphere [5]. Shortly thereafter in 2015, the then IMAG PhD student David Bernard replicated the Martian CO₂-dominant atmosphere within "La Planeterrella" and subsequently observed a visible blue Aurora, whose shape further confirmed MAVEN's findings [6].

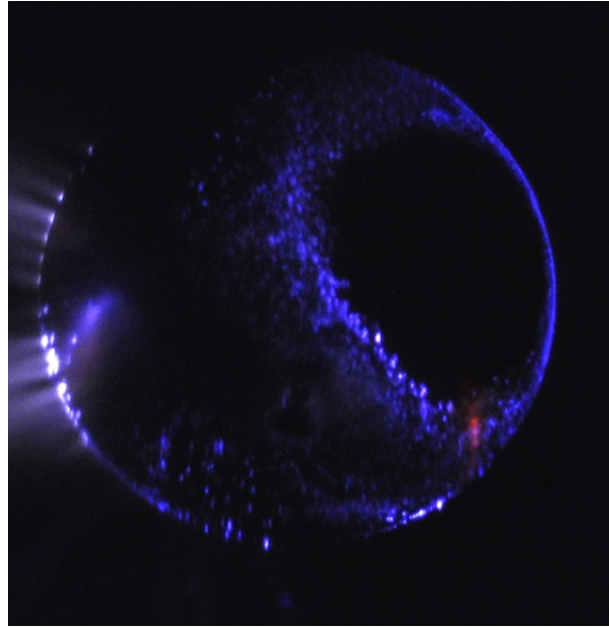


Figure 2.1: Bernard's experimental Planeterrella results for modeling the Martian atmosphere. Note the blue color and orientation of the produced aurora.

In addition, the IMAG team is using "La Planeterrella" to visualize how ring currents form around planets which possess a magnetic field on a tilted axis[6].

Chapter 3

Motion of Charged Particles in Electric and Magnetic Fields

The single particle motion theory of plasma was used to model the Ring Currents in the Planeterrella. In this framework, plasmas are represented by their constituent ions and electrons as test particles, ignoring their interactions. The motion of these particles is dictated by the presence of electric and magnetic fields. The action of these fields is described by applying Newton's second law to electrons experiencing the Lorentz force. The dynamics of the ions in the chamber are ignored due to both their short lifespan, wide cross section, and their large mass. This chapter lays down the mathematical formalism and concepts behind how electromagnetic effects govern the behavior of ring currents.

3.1 The Lorentz force and pertinent plasma parameters

Single particle motion entails viewing a plasma as an assembly of charged particles, the motion of each solely dictated by the electric and magnetic fields. This approximation initially neglects particle interactions, which are modeled in a collision algorithm discussed in chapter 4.

Charged particles in an electromagnetic fields experience the Lorentz force:

$$\vec{F} = m \frac{d\vec{v}}{dt} = q(\vec{E} + \vec{v} \times \vec{B}) \quad (3.1)$$

Where q is the charge of the particle in consideration, \vec{v} is its velocity at a given moment, \vec{E} is the electric field and \vec{B} is the Magnetic field. The expression between \vec{v} and \vec{B} is known as the cross product of two vectors and will yield a third vector perpendicular to the first two. Due to this, the

magnetic force $q(\vec{v} \times \vec{B})$ will always be perpendicular to the particle's velocity, resulting in circular motion unless acted on by another force. This orbital motion is known as *cyclotron motion*. The center of the cyclotron orbit is called the *guiding center*. On the other hand, the electric force $q\vec{E}$ will either move a particle along or against its orientation if the sign of the charge is positive or negative, respectively. The two most significant parameters describing the motion of a charged particle within a magnetic field are the Larmor radius and frequency (also known as the cyclotron radius/frequency). Qualitatively, the Larmor radius describes the radius of the orbital motion exhibited by a moving charged particle, and the Larmor frequency dictates how long it takes for the particle to complete said orbit.

The Larmor frequency is given by the following equation:

$$\omega_c \equiv \frac{|q|\vec{B}}{m}, \quad (3.2)$$

where m is the mass of a charged particle. Its spatial counterpart, the Larmor radius is given by:

$$r_L \equiv \frac{v_{\perp}}{\omega_c}, \quad (3.3)$$

where v_{\perp} is the velocity of the particle perpendicular to the orientation of the magnetic field.

3.2 Guiding center particle drifts

For a plasma in a uniform electric and magnetic field, the Lorentz force encodes all of the information necessary to describe the motion of its constituent charged particles. In the Planeterrella, a radial electric field is created due to the potential difference between the -2kV biased sphere and the grounded surrounding bell jar, and a dipole magnetic field is created by the 0.5T bar magnet embedded within the sphere. When there are perpendicularly oriented magnetic and electric fields, trajectories of the charged particles begin to exhibit *guiding center motion*, in which the center of the particle's cyclotron orbit moves over time. When there is spatial variance in the magnetic field, additional drift velocities are observed. In order to describe electron motion due to the electric and magnetic dipole fields within the Planeterrella, three new concepts must be introduced, the $\vec{E} \times \vec{B}$ drift, the magnetic gradient and the curvature drifts.

3.2.1 $\vec{E} \times \vec{B}$ drift

The primary driver of the orbital motion in the Planeterrella, the $\vec{E} \times \vec{B}$ drift, arises from perpendicularly oriented electric and magnetic fields. The electric field accelerates the particle during one half of the cyclotron orbit and decelerates it during the other half due to its orientation. This creates anomalies in the cyclotron orbits of the particles, since the Larmor radius is different on one half than the other. What results is a net movement of the guiding center of the particle perpendicular to both the electric and magnetic fields. In the Planeterrella, the $\vec{E} \times \vec{B}$ drift is due to the radial electric field and the upward oriented magnetic dipole field. This guiding center velocity is given by:

$$\vec{v}_{\vec{E} \times \vec{B}} = \frac{\vec{E} \times \vec{B}}{|B|^2} \quad (3.4)$$

Note that this velocity does not depend on the mass or charge of the particle, so no net current arises. In a moving frame with this velocity, there is no electric field. This drift causes ions in the Planeterrella to move in $\hat{\Phi}$, orbiting the sphere. Below is an illustration of $\vec{E} \times \vec{B}$ drift motion.

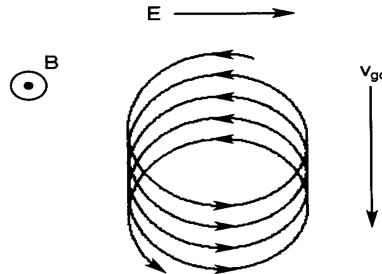


Figure 3.1: Depiction of guiding center drift due to perpendicular electric and magnetic fields. Here, the magnetic field is oriented into the page, and the electric field is oriented to the right. The direction of the guiding center motion is denoted by v_{gc} . [7]

3.2.2 Magnetic gradient ($\nabla \vec{B}$) drift

For this treatment, we assume that the spatial variation in the magnetic field is small with respect to the Larmor radius, characterized by

$$\frac{r_L}{B} |\nabla B| \ll 1. \quad (3.5)$$

This is applicable for the electrons within the Planeterrella, and an assumption to be made moving forward to derive our guiding center drift. The *gradient*, denoted by ∇ is a differential operator that yields a vector containing the spatial derivatives of the object it operates on. When there are spatial variances of the magnetic field, another charged particle motion arises called the *magnetic gradient drift*, which has a velocity given by

$$\vec{v}_{grad} = \pm \frac{v_{\perp}^2}{2\omega_c} \frac{\vec{B} \times \nabla \vec{B}}{|B|^2} \quad (3.6)$$

Since this velocity is dependent upon the charge (by virtue of its Larmor frequency dependence), ions and electrons will have opposing velocities. These opposing velocities are indicated by the plus or minus symbol for ions or electrons, respectively. These opposing motions result in a net current.

3.2.3 Magnetic curvature drift

In order to establish another guiding center drift, an additional assumption must be imposed. Locally, the magnetic field has a constant strength with respect to time, and the magnetic field lines have a radius of curvature R_c . With this assumption in place, it can be shown that charged particles will experience a radial *centrifugal pseudo – force*, given by

$$\vec{F}_{cf} = \frac{mv_{\parallel}^2}{R_c} \hat{r}, \quad (3.7)$$

where v_{\parallel} denotes the charged particle's velocity parallel to the magnetic field's orientation. While there is also theoretically a "Coriolis pseudo-force" experienced by the particle, it has zero magnitude and thus need not be considered. The presence of the centrifugal pseudo-force will result in another guiding center drift, the *curvature drift*. This drift velocity is given by

$$\vec{v}_{curv} = \pm \frac{v_{\parallel}^2}{\omega_c} \frac{\vec{B} \times \nabla \vec{B}}{B^2}, \quad (3.8)$$

where the plus or minus symbol again corresponds to ions and electrons, respectively.

3.3 Magnetic dipole fields

With the knowledge of the motion of charged particles in electromagnetic fields in place, we can now return to the main goal of characterizing electron motion within the Planeterrella. If

we use a Cartesian coordinate system and assume that our magnetic dipole is oriented in the \hat{z} direction, then the magnetic field at any location (x, y, z) is given by:

$$\vec{B}_{dipole} = \frac{3Mxz}{r^5}\hat{x} + \frac{3Myz}{r^5}\hat{y} + \frac{M(3z^2 - r^2)}{r^5}\hat{z} \quad (3.9)$$

Where M refers to the magnetic dipole moment. In the case of the Planeterrella, the M is given by

$$\vec{M} = \mu_0 \vec{B} \times 2l = 1.26 \times 10^{-6} \frac{mkg}{As^2} \times (5 \text{ Tesla}) \times (2 \times 0.05m) = 6.3 \times 10^{-7} \text{ Joules/Tesla.} \quad (3.10)$$

For the Planeterrella's configuration, we estimate the radius of curvature to be 5 cm based on the geometry of the Bell Jar, and apply equation (3.7) to find an expression for the curvature drift velocity of an electron in the Planeterrella's magnetic dipole field,

$$\vec{v}_{curvature,dipole} = \frac{-6W_{\parallel}}{eBr}\hat{\Phi}. \quad (3.11)$$

Where W_{\parallel} denotes the parallel kinetic energy of the electron, $\frac{m_e(v_x^2 + v_y^2)}{2}$. For the gradient drift velocity of an electron in the Planeterrella's magnetic dipole field, we apply equation (3.5) to find

$$\vec{v}_{gradient,dipole} = \frac{-3W_{\perp}}{eBr}\hat{\Phi}. \quad (3.12)$$

Where W_{\perp} denotes the perpendicular kinetic energy of the electron, $\frac{m_e(v_z^2)}{2}$. To analyze the motion of charged particles in this configuration, we will introduce some new quantities for convenience.

The *pitch angle* is given by the following relation:

$$\alpha = \tan^{-1}\left(\frac{v_{\perp}}{v_{\parallel}}\right) = \tan^{-1}\left(\frac{(v_x^2 + v_y^2)^{1/2}}{v_z}\right). \quad (3.13)$$

The pitch angle can also be thought of as the angle of the particle's velocity with respect to the magnetic field line. Another quantity of interest is a *magnetic mirror point*, or a point where the strength of the B field is high enough to make a particle reverse its velocity component parallel to \vec{B} . This reversal occurs when the pitch angle is 90 degrees.

In the case of a dipole field, there are both particles gyrating along the field lines exhibiting bounce motion between the the polar magnetic mirror points, as well as particles orbiting about

the center in the equatorial plane. Since both the curvature and the gradient drifts are in the $\hat{\Phi}$ direction, they play a key role in the formation of ring currents. Examples of charged particle trajectories in Earth's magnetic field are shown below.

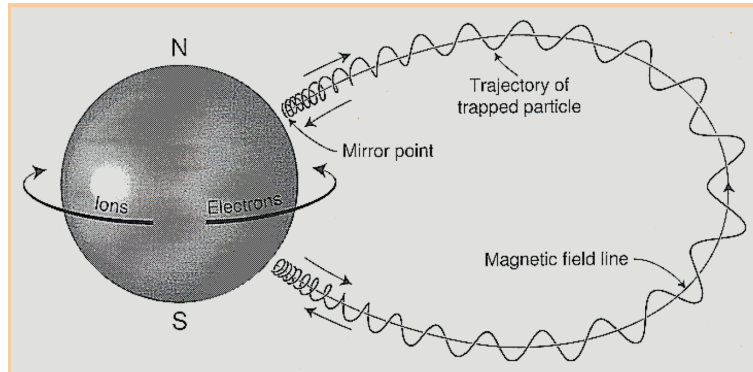


Figure 3.2: Charged particle motion about the Earth. The ring current motion due to curvature and gradient drifts closer to the Earth for ions and electrons is indicated, as well as gyration about magnetic field lines and bounce motion between polar magnetic mirror points. Credit: NASA/GSFC

Chapter 4

Collisional Phenomena

A plasma whose collision frequency is much greater than its cyclotron frequency is considered collisional. For a plasma with highly collisional regions such as those producing light in the Planeterrella, interparticle collisions play a quintessential role in determining their behavior. They are responsible for the energy transport, excitation and recombination processes. The number of collisions that occur per unit time is the *collision frequency*. The light produced by a Planeterrella device is due to photons being emitted from excited atoms after a collision with a sufficiently energetic electrons. Due to this, characterizing the collision profile in the chamber will reveal the patterns of light witnessed in the laboratory. In this chapter, a basic theory of collisions is established within the context of the Planeterrella.

4.1 Key parameters

For a relatively cool plasma, we may assume the ion and electrons exhibiting the motion described in chapter 3 are ideal spheres. The *cross section*, σ , between two particle species is simply defined as the area of a circle whose radius is the sum of the radii of the constituent spheres:

$$\sigma = \pi(r_1 + r_2)^2, \tag{4.1}$$

where r_1 and r_2 represent the respective radii of the two species colliding. For the purposes of the Planeterrella we are only concerned with the collisions between the electrons and neutral N₂ and O₂ atoms (for reasons explained more in depth in the next section). Therefore, in our model

a cross section of $\sigma = 0.025 \times 10^{-16} \text{ m}^2$ is implemented for all collisions, directly calculated from the measurements in [8]. If we denote the density of particle species α with n_α , then an additional quantity of interest is the *mean free path length*, λ_{mfp} , the average distance traveled by the species between collisions. The mean free path length is given by

$$\lambda_{mfp} = \frac{1}{(\sigma n)}, \quad (4.2)$$

where σ and n describe a specific particle species' cross section and density. Each of the above defined quantities are demonstrated in the below figure:

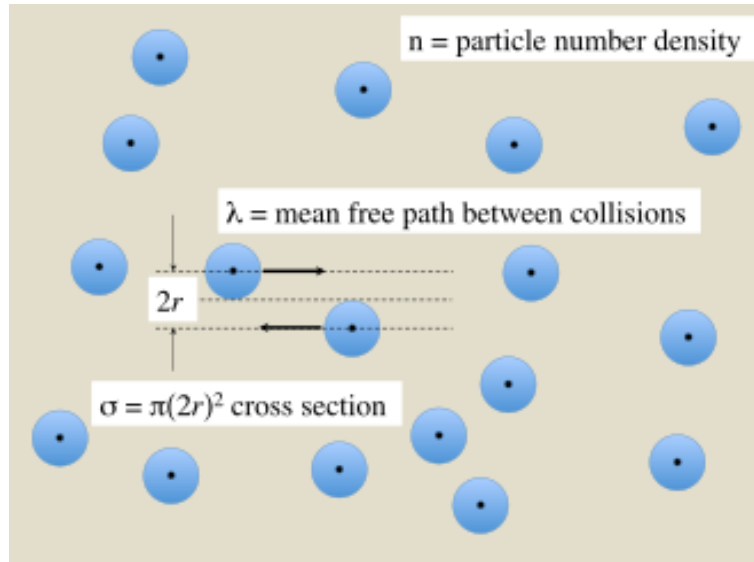


Figure 4.1: Representations of the density, cross section and mean free path length for an arbitrary particle species.

A final quantity of use is the *collision frequency*. If we assume all particles are moving with an average velocity v , then the collision frequency is defined as:

$$\nu_{\text{collision}} = \sigma n v. \quad (4.3)$$

Due to their dependence on n and σ , the mean free path and the collision frequency are inversely related to each other. Physically, this means that when there are more frequent collisions, the particles move less in between each impact. Less time between collisions means that they have less time to experience acceleration due to electromagnetic forces, so in turn the average velocity

will decrease as well. This is why the Planeterrella only produces light when pumped down within the vacuum chamber.

4.2 Impact excitation

Since the visible rings in the Planeterrella are due to photon emission of excited neutral atoms, incorporating impact excitation within our model is essential. The process of electron-impact ionization between a free electron and a neutral atom is described as follows:

- 1) A free electron with a kinetic energy higher than the binding energy of the neutral atom collides, freeing another electron from its valence belt in the process.
- 2) The neutral atom is now in a metastable state in which it is simultaneously ionized and excited. This state generally has a lifetime of 10 nanoseconds. There are now two free electrons, the initial one and the one that has been removed from the atom.
- 3) If the ionized atom collides with an electron during its 10 nanosecond lifetime, *recombination* occurs, in which the free electron combines with the ion, returning it to its neutrally charged state.
- 4) Regardless of whether or not the ion experiences recombination with a free electron, after 10 nanoseconds the excited ion/atom will emit a photon of energy equal to the difference between its excited and ground state energy levels, remaining ionized.

Electron-impact excitation in which recombination does not occur is described by the following particle equation:



where electrons are denoted by e^- , A represents the neutral atom, A^* represents the excited and ionized state, and A^+ describes the resultant ion, $h\nu_p$ represents the energy of the emitted photon, where h is Planck's constant = 6.626×10^{-34} m² kg/s, and ν_p represents its frequency. Since

the photon's energy directly depends on the frequency ν_p , “purple” photons have higher energy than their “red” counterparts, according to the electromagnetic spectrum. The ejection of these additional free electrons is the reason behind the continuous light in the Planeterrella. These ejected electrons can excite other neutral molecules, leading to a spread of neutral molecules emitting photons in a phenomena known as an *electron avalanche*.

4.3 Excitations

In order to accurately predict the behavior of impact excited ions, the type of excitation they experience upon collision must be described. In order to provide this description, we rely on the use of quantum mechanics. Here, the energy of an atom is given in discrete levels, or *quanta* instead of a continuous regime of energies like in the classical framework. The type of excitation will vary based on environment and collision. The most common excitations witnessed within plasmas are rotational and vibrational. In vibrational excitations, the atom's energy behaves like that of a quantum harmonic oscillator, jumping between energy levels with a given magnitude.

4.3.1 Rotational excitations

Rotational excitations are the most common within plasmas and are the dominant excitation present in the Planeterrella [9]. In this model, we simplify our neutral N₂ and O₂ molecules as *rigid rotors*, where the N and O atoms are point masses connected by their bond, which is simplified to a stiff beam. The energy of this system is described with the quantum internal Hamiltonian

$$H = \frac{\hbar^2}{2I} \left(\frac{\partial^2}{\partial \theta^2} + \frac{\partial^2}{\partial \phi^2} \right), \quad (4.5)$$

where \hbar is Planck's reduced constant = 1.054×10^{-34} J s, θ is the elevation angle and ϕ is the azimuth. I is the moment of inertia, which is proportional to the mass of the atoms and the square of their equilibrium bond length. The moment of inertia for N₂ is 2.6×10^{-46} kgm², and O₂ is 1.95×10^{-46} kgm² [?].

The application of *Schrödinger's Equation* to this Hamiltonian yields the quanta of angular momentum energy states

$$E_r = \frac{\hbar^2}{8\pi^2 I} J(J+1), \quad (4.6)$$

where J is the total angular momentum quantum number. In this model the different energy levels can be thought of as the quanta of speeds and orientations that the rigid rotor can rotate with. The first excited state of Oxygen is known as the singlet state. High concentrations of Oxygen have been observed to glow at 650 and 703 nanometers, which is the wavelength of visible red light [?, ?]. Similarly, the first excited state of Nitrogen gas (N_2) has been observed to glow with visible purple light [1]

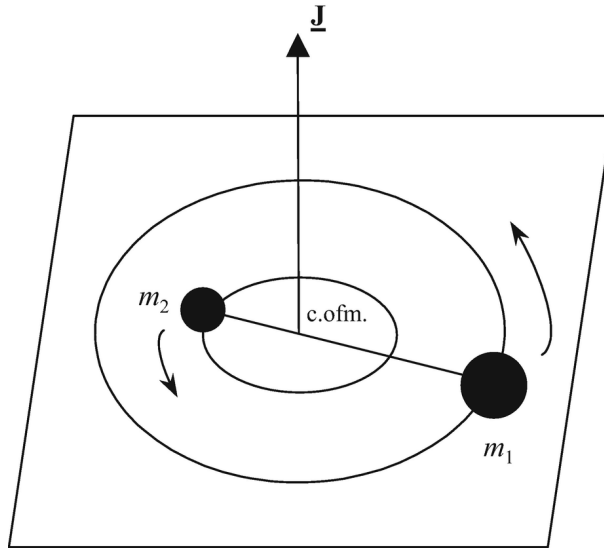


Figure 4.2: Artist's rendering of a quantum rigid rotor. For the N_2 and O_2 molecules within the Planeterrella, $m_1 = m_2$. Here, c.ofm. is short for the center of mass, and the orientation of the quantum total angular momentum J is indicated.

With this, the physical model of the Planeterrella is complete: Free electrons are ejected from a biased sphere, where they exhibit Larmor gyration, bounce and curvature/gradient drift motion due to a magnetic dipole field and a weak radial electric field. Throughout this motion, they collide with and excite neutral N_2 and O_2 molecules, which in turn emit the photons witnessed by the observer.

Chapter 5

Construction of the Experimental Apparatus

This chapter describes the construction of the Planeterrella device built at LASP/IMPACT by Robert Varrennes under the supervision of Professors Mihály Horányi and Xu Wang in 2017. Below is a summary of the construction process and a description of the different components of the apparatus.

5.1 SolidWorks model

The structural components of the Planeterrella apparatus are shown in Figure 5.1. In order to relay the correct dimensions of the different components to a vendor for manufacturing, accurate drawings are produced as indicated in Figure 5.1. The rendered SolidWorks model of the glass bell jar mounted on the aluminum baseplate is also shown in Figure 5.1.

The bell jar and baseplate are imperative to the experiment, as they provide low pressure

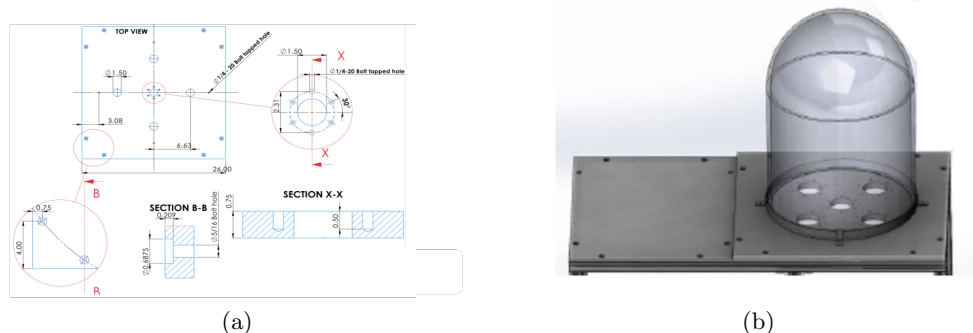


Figure 5.1: a) Aluminum baseplate diagram of the Planeterrella apparatus and b) Solidworks rendering of the bell jar, vacuum seal and the baseplate of the Planeterrella apparatus.

for excitation. The inside pressure is set within a range of 500-750 mTorr, achieved by the vacuum setup which is built around a mechanical pump. The vacuum chamber is a 40.64 cm diameter and 63.5 cm tall bell jar resting on a 1.9 cm thick aluminum base and sealed with a Viton o-ring.

5.2 Mechanical fabrication

To produce a magnetic field around a sphere, a strong cylindrical neodymium magnet is installed vertically inside the center of a hollow sphere. The hollow sphere is made of aluminum and consists of two hemispheres of outside radius of 2.54 cm and a wall thickness of 0.5 cm. The mating halves are threaded together and register to one another using a 0.254 cm deep inner step as illustrated in Figure 5.2. The sphere stands on an insulating tube which is secured at the baseplate. An electric wire is routed through the tube and is connected to the sphere.



Figure 5.2: The two mating aluminum hemispheres.

The mounting tube is secured to the center of the base plate using six $\frac{1}{4}$ -20 bolts. The bolts use tapped holes located on a 5.87 cm diameter circle located around the 3.81 cm feed-through center hole. Finally, linear and rotary translation of the magnet can be achieved using mechanical adjuster secured to the frame of the assembly under the baseplate as illustrated in Figure 5.3. Vacuum down to about 5 mTorr may be produced using a pump assembly placed under the baseplate. The pressure in the chamber is tuned by bleeding air through a leak valve, achieving a resolution of 1 mTorr. Schematics of the pumping system to create a vacuum in the jar is shown in Figure 5.4. The system was kept clean during assembly to prevent leaks. Cleaning agents such

as ethanol and acetone were used for the task which took several iterations to achieve leak-free assembly. After fabrication and assembly, the resultant functional vacuum system is shown using the views in Figure 5.4.



Figure 5.3: Linear and rotary position adjustment of the magnet.



Figure 5.4: a) Vacuum system diagram and b) Implemented vacuum system.

5.3 Electric system

The electrical subsystem consists of the electrodes, generator and the sphere containing the magnet. the high voltage power supply is connected the baseplate, which is grounded. The high voltage passes through a strong $0.5 \text{ M}\Omega$ resistor in order to mitigate excess current. Finally, a power generator is fixed to the frame of the assembly, and the setup is grounded to avoid charge accumulation on the plate. A schematic of the electric connections is illustrated in Figure 5.5.

To adjust the magnet in both translation (up-down) and rotation in the $\hat{\phi}$ direction, a vacuum-compatible rotary motion which can fit a 1/4" OD tube is installed (see Figure 5.3). These resulting degrees of freedom allow us to axially alter the dipole field produced by the bar magnet for exper-

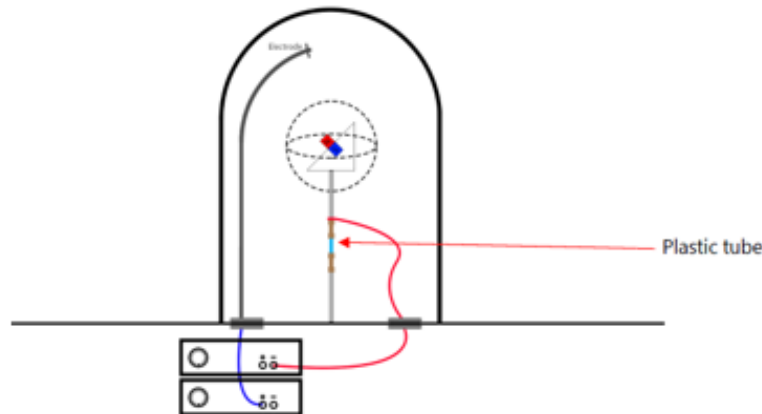


Figure 5.5: Schematics of the electric connections.

iments on tilted magnetospheres. The magnet holder and the lower hemisphere both have a 1/4" taped hole to fit on the tube.

The tube is divided into 2 parts to be able to dismantle only the part with the sphere when doing adjustments. The two tubes are connected with a brass adaptor. The final implemented electric system is shown in Figure 5.6.

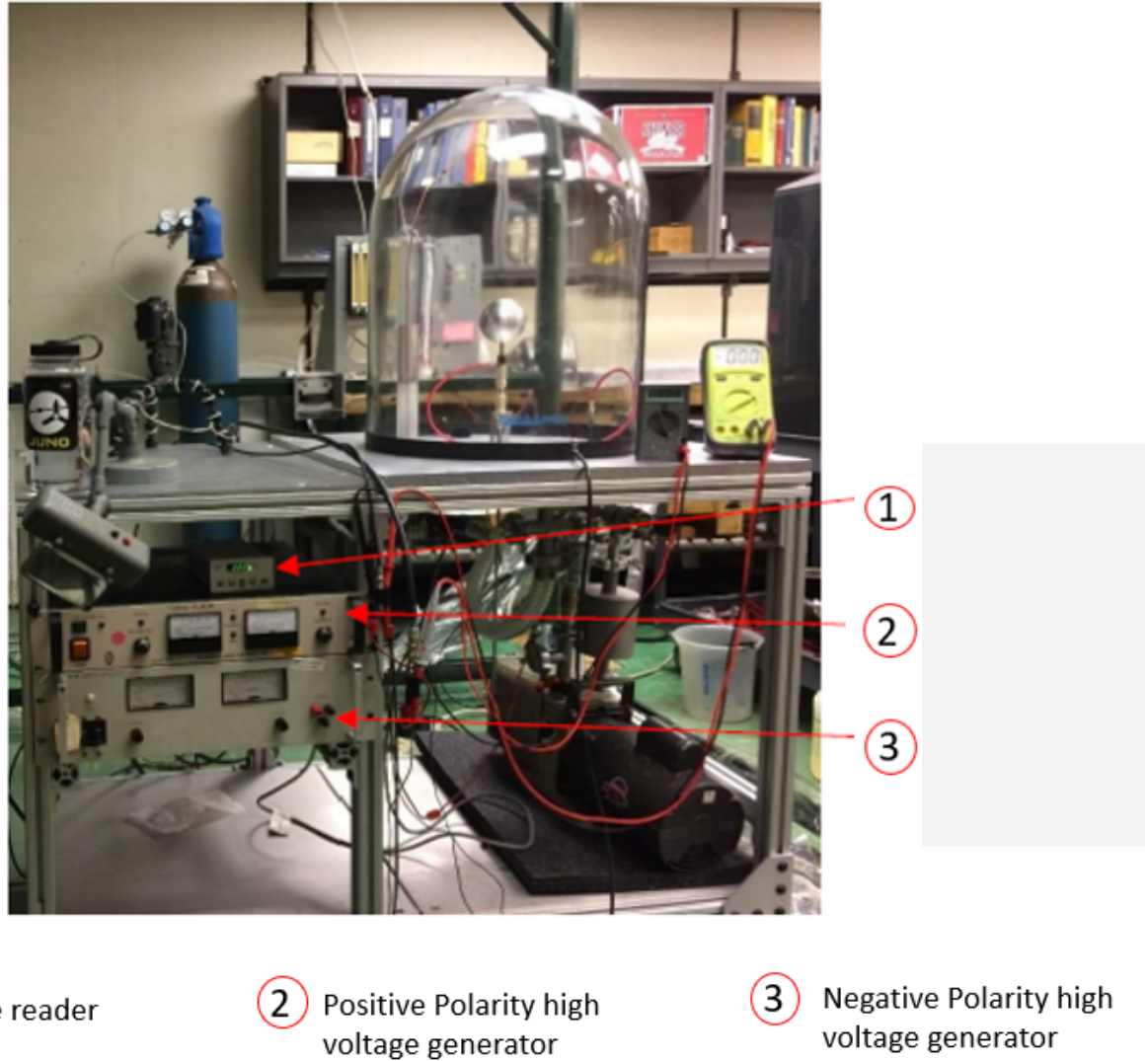


Figure 5.6: Auxiliary components in the electrical system.

Chapter 6

Simulation

The most recent contribution to the Terrella project was the first successful implementation of software to follow charged particles in the Terrella's physical system. A fourth order Runge-Kutta-based Monte Carlo Collision algorithm was developed in the Python programming language to model the physical phenomena described in chapters 3 and 4. Its development and implementation are discussed in this chapter.

6.1 Runge-Kutta numerical integration

The trajectories of the charged particles are determined by repeatedly feeding in updated position and velocity initial conditions into a Lorentz Force integrator that is prescribed the Cartesian equations of the magnetic dipole field and weak radial E-field within the Planeterrella in the Python routines. This iterative method is known as a *fourth-order Runge-Kutta* integrator [?].

6.2 Python implementation

The means to implement a Runge-Kutta integrator of order 4 in Python is encoded within a function named *odeint* from the Python library **Scipy**. In the implementation for the LASP/IMPACT Planeterrella, our Runge-Kutta function $f(t)$ is the differential equation for motion dictated by the Lorentz force. The initial conditions "fed" in each iteration are the position and velocity from the previous timestep, this data is encoded within "numpy arrays" from the Python library **Numpy**.

For a given timestep i , the equation being solved with the Runge-Kutta method is:

$$\frac{d\vec{v}_{i+1}}{dt} = \frac{q}{m}(\vec{E}_i + \vec{v}_i \times \vec{B}_i) \quad (6.1)$$

Equation (6.2) is a discretization of equation (3.1). In our implementation, we first define $r_i = \sqrt{x_i^2 + y_i^2 + z_i^2}$. Then, we update the dipole magnetic field periodically based on the following vector discretized equations:

$$\begin{aligned} B_{x,i+1} &= \frac{3*M*x[i]*z[i]}{(r_i^5)} \\ B_{y,i+1} &= \frac{3*M*y[i]*z[i]}{(r_i^5)} \\ B_{z,i+1} &= \frac{M*(3*z[i]*z[i]-r_i^2)}{(r_i^5)}. \end{aligned}$$

The above equation is a discretization of equation (3.8). Whereas with the electric field, it is radially inward with a $\frac{1}{r^2}$ dependence:

$$\vec{E}(x_i, y_i, z_i) = \frac{-V_S}{0.02(x_i^2 + y_i^2 + z_i^2)} \hat{r} \quad (6.2)$$

The electric field was calculated by solving Poisson's equation within the vacuum chamber. Since we are only interested in the motion in the equatorial plane, we impose the assumption that the system is cylindrically symmetric. Additionally, we require that the sphere is perfectly biased at 2kV and that the chamber is grounded. Therefore, the electric field was found by taking the negative gradient of the potential $-\nabla V$. V is given by $\nabla^2 V = 0$ and the boundary conditions inherent in our assumptions.

Based off of our framework established in chapter 3, this is essentially all that's needed to follow the motion of particles within the Planeterrella. The simulation was tested by recreating known dipole trajectories. The one pictured below is a direct analog of figure (3.1).

6.3 Simulation modeling of electron-impact excitation collisions

The probability of a collision between free electrons and neutrals is described by [3]:

$$P = 1 - e^{-n_s \sigma v dt}, \quad (6.3)$$

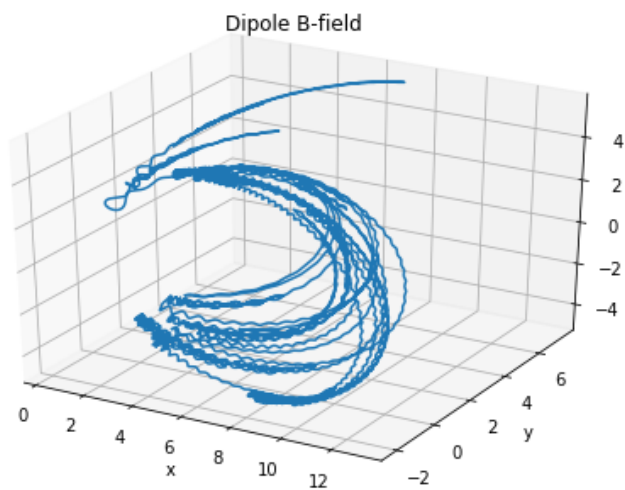


Figure 6.1: Simulation result for a particle gyrating along a magnetic field line, exhibiting bounce motion between two mirror points.

where n_s is the density of neutral molecules s , v is the velocity of the particle at the given timestep, dt is the amount of time between time steps, σ is the cross section between an electron and neutral N₂ given in chapter 4, $\sigma = 0.025 \times 10^{-16} \text{ m}^2$. The Monte Carlo Collision (MCC) method consists of comparing this probability to a uniform random variable that's randomized every time step. A collision occurs if the probability from equation (6.5) is higher than that of the random variable.

When there is a collision, the incident kinetic energy of the electron is given by:

$$T_i = \frac{m(v_{x,i}^2 + v_{y,i}^2 + v_{z,i}^2)}{2}. \quad (6.4)$$

6.3.1 Modeling photon emissions

What we set out to show is that the two discrete rings formed in the Terrella are due to the two different molecules experiencing impacts. In order to analyze the light produced by the Terrella, we have to compare this incident kinetic energy to the ionization energy of N₂ and O₂. The ionization energy of N₂ is $15.58 \pm .008 \text{ eV}$, and the ionization energy of O₂ be $12.07 \pm .0002 \text{ eV}$ [13]. Using these quantities, the simulation separates each collision with the following algorithm:

- 1) If $T_i < 12.07 \text{ eV}$, we assume an elastic collision, simply inverting the velocities on the next time step: $v_{x,i+1} = -v_{x,i}; v_{y,i+1} = -v_{y,i}; v_{z,i+1} = -v_{z,i}$. This does not propagate unreasonable error since the mass of N₂ and O₂ is so much higher than that of an electron.
- 2) If $12.07 \leq T_i \leq 15.58 \text{ eV}$, then O₂ is impact excited. This means that we *recursively* call our integrator within itself, so we start following the trajectory of another electron at that moment, in addition to following the existing one. This recursively spawned electron models the extra free electron on the right hand side of equation (4.4). The energy of these electrons is distributed as follows: we subtract 12.07 eV from T_i of the incident electron, then we use 6 uniform random variables that add to 1 in order to randomly redistribute the remaining energy amongst the two electrons in x,y and z. If these electrons don't experience another collision after 10 nanoseconds (how many timesteps this is will be determined by

the size of the timestep defined by the user) a red point is plotted to emulate Oxygen's emission of a photon. The location of this point is the same location as the collision for simplicity. If another collision *is* experienced within the 10 nanoseconds, then we emit the photon at the following timestep.

- 3) If $T_i > 15.58 \text{ eV}$, then N_2 is impact excited. This will follow the same process described in step 2, but an energy of 15.58eV is subtracted from the incident electron, and a purple photon is emitted instead. The same process follows for O_2 if $T_i > 12.07 \text{ eV}$.

An assumption inherent in this algorithm is that 1) the electrons, ions and neutrals all behave ideally, and that 2) N_2 and O_2 are only excited to one state. This is the state whose energy is exactly larger than the ground state by the energy of a Purple and Red photon, respectively. The energy of these states is given by equation (4.6).

Once the simulation completes, a 3-dimensional plot of the collisional profile is produced. Plotting for this simulation is handled with the **Matplotlib** Python library. An example result is shown in figure (7.1).

6.4 Parallelization

The long run time of the simulation was curtailed via the implementation of parallel processing in the code. This was handled with Python's **Multiprocessing** library. The Multiprocessing library is an implementation of *Process-Based Parallelism*, in which an iterative process is divided amongst the computer's processors. The way it does this is that processes are passed into a queue to be processed simultaneously and when the processes finish their outputs are sent into a data pool upon completion. This practice is especially useful in supercomputer simulations, in which processes number in the thousands, yielding incredibly high performance computing. See figure 6.2 for an illustration of the multiprocessing algorithm.

The benefit of including this practice in the Planeterrella simulation was that 8 particles could be simulated at once rather than one. The reason 8 particles ran concurrently was that the

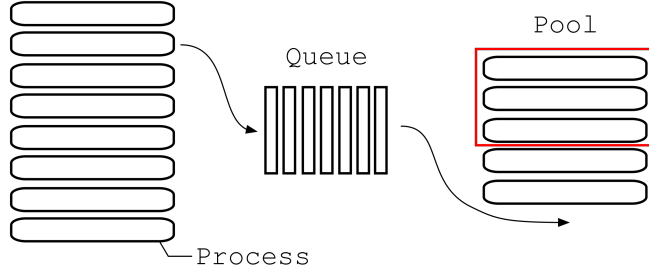


Figure 6.2: Illustration of the multiprocessing algorithm when implemented over 8 cores. Credit: Konstantin Taletskiy, towardsdatascience.com

simulations were carried out on computers with 8 cores. The usual runtime of 200 particles for 100 billion nanosecond timesteps (100 seconds total of simulation time) took around 32 hours on average. The output, collision locations for Nitrogen or Oxygen excitations, was gathered and processed via creating "dataframe" objects of each particle and processing them via Python's **Pandas** library.

6.5 Collision density analysis

In order to further analyze the Planeterrella's ring currents, an analysis of the relationship between collision density and luminosity was also conducted. Within the simulation, the equatorial X-Y plane was isolated as a discrete set of grid points. Whenever a collision occurred, its (X,Y) location is stored. In order to calculate the density, we once again turn to a function within Python's **Scipy** library.

A *density estimator* is an algorithm that creates a histogram of provided data points. This histogram gives a probabilistic distribution of the data being input. For the case of the Terrella, we input the number of collisions per (X,Y) location, then create a histogram from it.

The method implemented for modeling the collision density of the ring currents is known as a *Gaussian Kernel Density Estimate*. The *kernel* is the shape of the distribution (the actual histogram data plotted), and the *kernel bandwidth* is the size of each histogram data point. This means that when there is a collision, we assume a Gaussian distribution nearby collisions and can

interpolate the nearby density values as a result. The result is shown in figure (6.2):

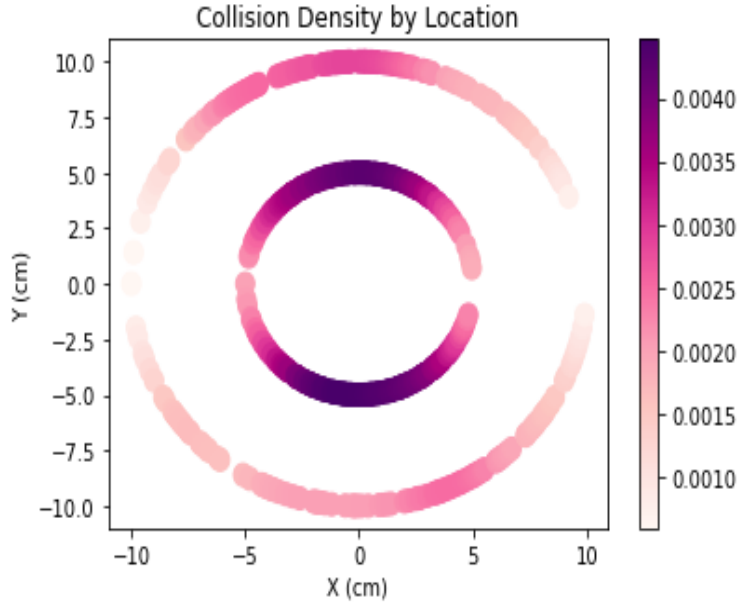


Figure 6.3: Density estimate results.

While the Kernel Density Estimation method is computationally expensive, it provides an accurate depiction of the birds eye view of the stellar ring currents and can give us insight into their luminosity. An additional luminosity estimation method is provided below.

6.6 Image luminosity analysis

In order to create trends of luminosity vs. collision density, we use the birds eye view pictures taken of the Terrella when it is producing the stellar ring currents. The way the brightness was analyzed was with the **Python Imaging Library (PIL)**. A function was developed that reads in the images as an array of pixels, then returns the root mean square of the brightness. Similar to the density estimation algorithm, a grid of each (X,Y) location is created, then a histogram brightness value is assigned to each grid point, or pixel in this case. Using this function, luminosity trends were established that are shown and discussed in Chapter 7.

Chapter 7

Results

It was shown via both simulation and experiment that the visible rings within the Terrella were due to the impact excitation of neutrals. This chapter entails a discussion of the simulation and physical experiments performed.

7.1 Simulation results

To simulate the ring currents, two hundred test electron particles were created. Simulating more particles was sacrificed in order to have more time steps per particle. More time steps were desired since the ring current orbits are on a longer timescale than cyclotron orbits. Their initial positions were created randomly around a circle and using a random number generator. The bright rings are reproduced by the Runge-Kutta simulation once the collisions are distinguished by their energies. These results are shown in figure 7.1. The simulated bright rings closely agree with the Planeterrella's in that the red ring is composed of fewer collisions and those collisions are further apart than that of the red ring.

In order to further characterize the rings, the collisional data in figure 7.1 was used to perform a kernel density estimate. The result is illustrated in figure 7.2. This estimate was not Gaussian, so no smoothing is applied.

To describe the speed of the electrons, the average velocity was calculated by location about the sphere in the equatorial plane. To do this, the equatorial plane surrounding the sphere was discretized into 22 radial and 61 azimuthal locations. When an electron passed through the location,

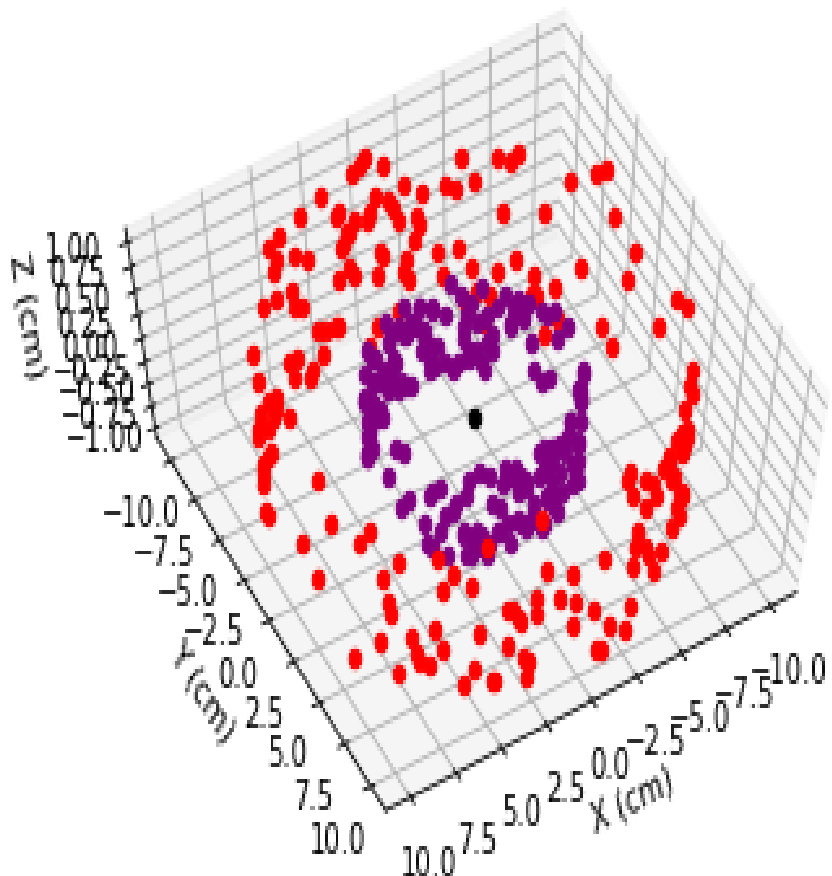


Figure 7.1: 3D collision profile for the ring currents. The black point represents the center of the magnetic dipole field. The gaps on the left and right hand side ($x = \pm 10$) are an artifact of the random numbers used to generate the y -values of both the positions and velocities of the radial distributions.

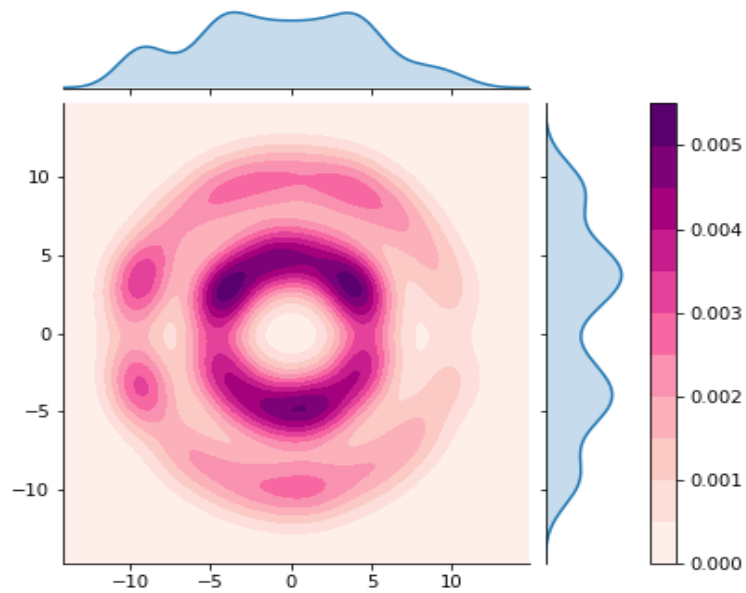


Figure 7.2: 2D density profile example for the stellar ring currents. The gaps on the left and right hand side ($x = \pm 10$) are an artifact of the random numbers used to generate the y-values of both the positions and velocities of the radial distributions. The histograms appearing on the opposite sides of the x and y axes represent probability distributions for the collisions based on location.

its velocity contributed to an average value. The results are given by figure 7.3.

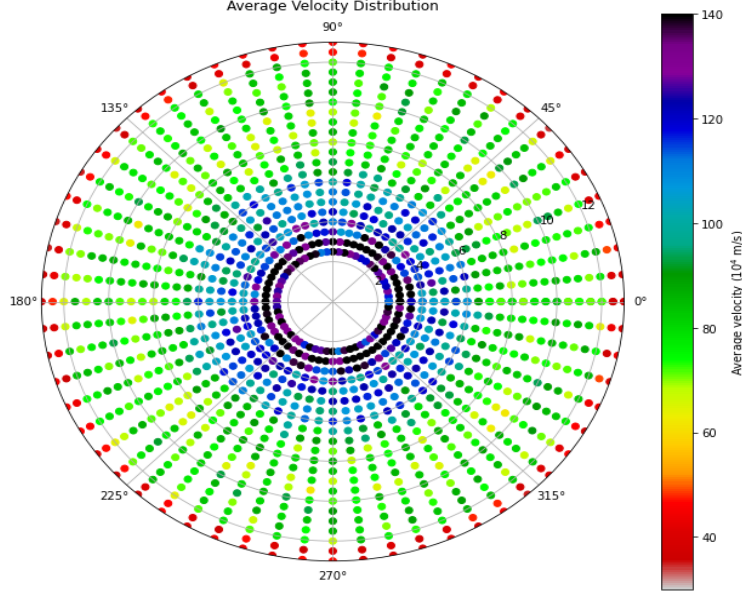


Figure 7.3: 2D average velocity distribution for up to 15cm from the center of the sphere. This is meant to represent a birds-eye view of the Planeterrella in a centimeter scale, where the colorbar represents the average velocity of particles in a given location. The uniformity in the data from 4-6cm and 8-12cm corresponds to the location of the rings. Note also that the scale is given in 10^4 m/s for better presentation.

These velocities were then used in conjunction with the dipole strength, cross section and density to produce the calculation for the ratio of electron cyclotron (gyro) frequency to collision frequency by location, given in figure 7.4.

Luminosity trends were established for Voltage dependence, using the methods described in section 6.6. The data was taken from when stellar ring currents *ignited*, or became visible, up to the high voltage power supply's arcing voltage of 2 kV. There were two trials (pictures taken) for each voltage. These results are described in table 7.1.

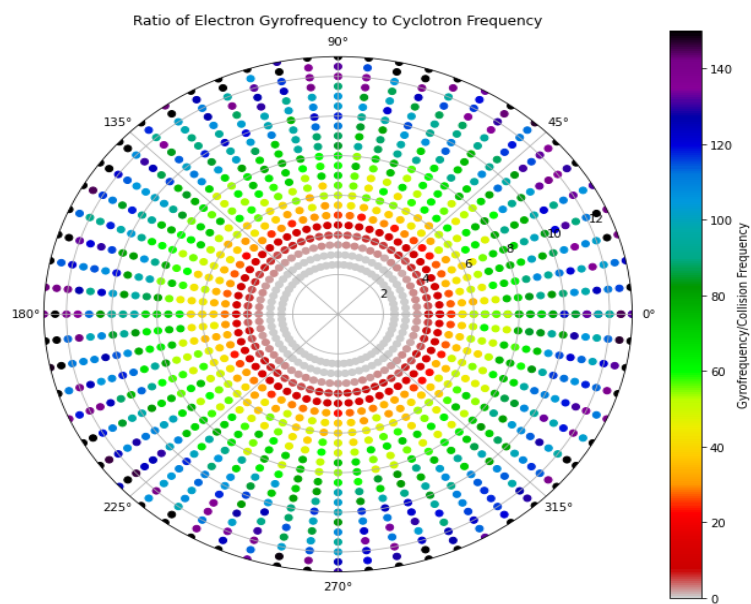


Figure 7.4: 2D average distribution of cyclotron frequency to collision frequency for up to 15cm from the center of the sphere. Here, the ratio is indicated by the color. This is again meant to represent a birds-eye view of the Planeterrella in a centimeter scale.

Table 7.1: Table of the ring luminescence results versus applied voltage and current run through the circuit. These measurements were taken from the ring current ignition voltage (800 Volts) to the largest voltage the high voltage power supply could handle before arcing (2000 Volts).

Ring Current Luminescence Averages				
Applied Voltage (Volts)	AC Current (mA)	Red Ring Brightness (L)	Purple Ring Brightness (L)	
800	1.6	56.3	64.2	
900	1.8	64.7	71.4	
1000	2	72.4	86.1	
1100	2.2	79.6	90	
1200	2.4	88.1	93	
1300	2.6	99.2	102.3	
1400	2.8	108.8	111	
1500	3	113.7	121.4	
1600	3.2	122	128.2	
1700	3.4	119	129.6	
1800	3.6	114	127.4	
1900	3.8	111	123.7	
2000	4	106.2	119.8	

Sources of error in the the results of Table 7.1 include error inherent in measuring the $5\text{ M}\Omega$ resistor, neglecting the resistance of the wires and any inconsistencies between the high voltage power supply's display and the voltage actually being delivered. In addition, the use of Python's Imaging Library to calculate the average brightness of the rings has its own sources of error. It Concerning these luminescence results, the Nitrogen experiment (described in section 7.2) was performed at 1600 Volts, produced the peak brightness for both rings.

7.2 Experimental results

To confirm that the composition of the gas determined the quanta of visible rings, the chamber was altered to vent out O_2 and pump in N_2 . This process entailed pumping down the existing gas within the chamber to 5 mTorr, then feeding in the pure N_2 and venting out the existing gas using the fine tuning valve pictured in figure (5.3). Once this process was finished, birds-eye view photos for all voltages after Ring Current ignition were taken. The results were exactly as expected, the Red ring disappeared. The result of running at 1600 Volts, the voltage where the Red ring was

most luminescent for normal air, is shown below.

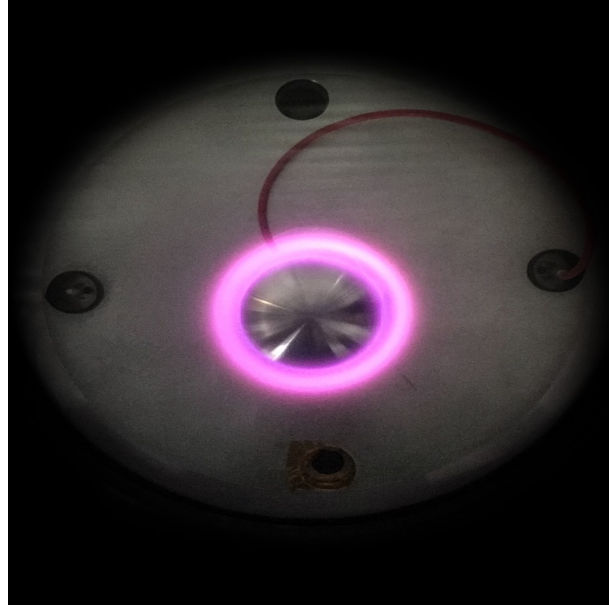


Figure 7.5: N₂ ring current result at 1600 Volts.

This result implies that the light produced by the Terrella is a spectra of the constituent gas. There are a discrete quanta of rings because electrons have drift velocities whose magnitude inversely depends on their radius from the center of the magnetic dipole field, as described in equations (3.10) and (3.11). This means that the electron-neutral collisions will be less energetic further from the sphere in the Terrella; therefore different ionization energies will be overcome at different distances from the sphere.

Chapter 8

Conclusion

A summary of findings is recounted, followed by possibilities for further research using the LASP/IMPACT Planeterrella and the accompanying numerical simulation.

8.1 Summary of Findings

A Planeterrella device was developed at LASP/IMPACT to visualize the behavior of charged particles (electrons) in planetary magnetospheres. Two discrete visible rings were produced using the Planeterrella using normal air within the chamber. To determine the source of these two regions of light, the air in the chamber was exchanged for pure N₂ gas, resulting in a single purple light ring within the chamber. A Runge-Kutta based Monte Carlo Collision (MCC) algorithm was developed to interpret the observed rings under the different test conditions. Several numerical simulations successfully reproduced the manifestation of these ring currents.

For the completion of this thesis I have run experiments and captured images of the light rings such as the one presented in Figure 7.5. Additionally, I have developed a Monte-Carlo collision simulation, and compared its predictions, e.g. presented in 7.1 and 6.3, to the laboratory measurements. The simulations and laboratory results were found to be in reasonable agreement.

8.2 Further research

8.2.1 Spectra based on different gas compositions

Experiments involving different compositions of gas could be used to establish a visible spectra of the Planeterrella's plasma. This is largely inspired by David Bernard's research on the Martian atmosphere using "La Planeterrella". An obvious choice of gas would be to pump out the existing air to 5 mTorr as was done for the Nitrogen experiment, then bleed in Oxygen gas until a pressure of 400 mTorr is reached. Care must be taken not to reach any higher pressure due to Oxygen's ease of combustion.

8.2.2 Tilted dipole field

The tilted stand for the sphere described in section 5.3 can be used to simulate ring currents and other plasma configurations for planets such as Uranus, whose magnetosphere is tilted to nearly 90 degrees. This would also enable studies of magnetic polar changes such as the one Earth has experienced in the past and is still happening today.

8.2.3 Improvements to the simulation

By making alterations to the existing Python code, the light witnessed in the Planeterrella can be more accurately represented by the simulation.

While the simulation described in chapter 6 was accurate enough to model the ring currents, improvements can be made to the simulation to more accurately model the more complex configurations. Firstly, translating the code from Python to a more computationally efficient language (C or Fortran) could greatly improve the statistics of these simulations.

These improvements could also include changing the integrator from a simple Runge-Kutta algorithm to a Boris integrator. The Boris integrator includes an error correction every timestep, whereas the Runge-Kutta accumulates slight error every cyclotron orbit. If a simulation includes a high number of cyclotron orbits, this error can accumulate and give rise to nonphysical results

such as artificial particle drifts. By implementing a Boris integrator, the plasma configurations of higher complexity can be more easily modeled in the simulation.

8.3 Glow Discharge

Another possible explanation for the visible ring currents would be a presence of a *Glow Discharge*, in which the voltage difference between a cathode and anode with gas in between them is sufficiently high such that ionization is sustained, yielding light due to recombination. Common examples of glow discharges include plasma screen televisions and neon lights.

If the glow discharge model accurately describes the Planeterrella, then the -2kV biased sphere would be the cathode, and the grounded cylinder the anode. The dark space between the rings would be the Faraday dark space, and the dark space outside the secondary ring would be the anode dark space. The key difference between the glow discharge model and the one described in this model is that glow discharge motion need not be adiabatic. This means that instead of drift motion being responsible for the light, it is simply the electric field between the cathode and anode driving it.

8.4 Research performed concurrently with this honors thesis

My second major project involves optimizing the Interstellar Dust Experiment (IDEX) instrument on Princeton's Interstellar Mapping and Acceleration Probe (IMAP) mission, which is a reflectron-style time of flight mass spectrometer that takes in-situ composition measurements of interstellar and interplanetary dust particles via electrostatic ion optics. My introduction to the optimization process involved familiarizing myself with SIMION, an industry standard simulation software for the motion of charged particles in electromagnetic fields. In order to meet Princeton's requirements for the instrument, a combination of Monte Carlo and Simplex optimization algorithms based on SIMION simulations of an accurate CAD model of the instrument is used. These results were presented in our principal design review, and have resulted in alterations to the instrument to boost performance. Findings from this activity will soon be published. Addition-

ally, I completed various information and technology (IT) tasks which consisted of readying a new computer for the dust accelerator here at IMPACT with data acquisition (DAQ) cards, drivers, and a Labview framework for instrument interface. The test setup which includes various scientific programming environments for data analysis.

Bibliography

- [1] W Benesch and J. Vanderslice. Excitation and photon emission rates of the auroral nitrogen first positive group. *Journal of Atmospheric and Terrestrial Physics*, 1:4–8, 1967.
- [2] R. Bernstein. Aurora demonstrations on the ui planeterrella. *Journal de Physique*, 1:1–12, 2016.
- [3] Lubos. Brieda. *Plasma Simulations by Example*. Taylor & Francis, 2019.
- [4] J. Butcher and G Wanner. Runge-kutta methods: some historical notes. *Applied Numerical Mathematics*, 1:1–4, 1996.
- [5] M. K. Elrod and B. Jakowski. Mars atmosphere and volatile evolution mission (maven). *Workshop on Volatiles in the Martian Interior*, 1819:1, 2014.
- [6] Lilensten et al. The planeterrella experiment: from individual initiative to networking. *Space Weather Space Clim.*, 1:1–6, 2013.
- [7] R. J. Goldston and P. H. Rutherford. *Introduction to Plasma Physics*. Taylor & Francis, 2000.
- [8] Winifred Huo. Electron-impact excitation and ionization in air. *NASA/NATO*, 1:3–20, 2008.
- [9] Yukikazu Itikawa. Cross sections for electron collisions with nitrogen molecules. *Journal of Physical and Chemical Reference Data*, 35:31–52, 2006.
- [10] Stanislaw Olbert and Bruno. Rossi. *Introduction to the Physics of Space*. McGraw-Hill Book Company, 1970.
- [11] K. Rypdal and T. Brundtland. Birkeland terrella experiments. *Journal de Physique*, 1:1–30, 1997.
- [12] J. K. Sandhu et al. Challenging the use of ring current indices during geomagnetic storms. *Journal of Geophysical Research: Space Physics*, 126, 2:all, 2021.
- [13] Y. T. Lee T. Trickl, E. F. Cromwell and A. H. Kung. State-selective ionization of nitrogen in the $x_2+gv+=0$ and $v+=1$ states by two-color (1+1) photon excitation near threshold. *The Journal of Chemical Physics*, 1:1–7, 1989.
- [14] D. A. Ranquist F. Bagenal R. J. Wilson. Polar flattening of jupiter’s magnetosphere. *American Geophysical Union*, 1:2–5, 2020.